This is my blah

A CLAS Proposal for PAC44

Transition Form Factors of the η' and ϕ Mesons with CLAS12

M. C. Kunkel*†[1], M. J. Amaryan[2], D. Lersch[1], J. Ritman†[1], S. Schadmand†[1], X. Song[1]

[1]Forschungszentrum Jülich, Jülich (Germany)
[2]Old Dominion University (U.S.A.)

Abstract

Dalitz decays are radiative decays in which the photon is virtual and subsequently produces an electron positron pair, $P \to l^+l^-X$. Such decays serve as an important tool used to reveal the internal structure of hadrons and the interaction mechanisms between photons and hadrons. Furthermore, assuming point-like particles, the electromagnetic interaction is calculable within QED by the Kroll-Wada formula. Transition form factors quantify deviations from the QED decay rate. They characterize modifications of the point-like photon-meson vertex due to the structure of the meson. For the η' meson this deviation represents the internal structure of the meson, while for the ϕ meson the deviation represents the transition from $\phi \to \eta$. The transition form factor can be characterized as $\left|F(q^2)\right|$, where q^2 is the square of the invariant mass of the lepton pair, and can be determined by comparing QED predictions to the experimentally measured rate.

Measurements with the highest scientific impact on the determination of the transition form factor have been performed in the space-like region ($q^2 < 0$) in collider experiments. However, due to experimental limitations (e.g. $\pi^\pm$ contamination in lepton sample, low branching fractions, external conversion contamination), transition form factors in the time-like region ($q^2 > 0$) have not yet been precisely determined. Recent measurements of the time-like transition form factor for $\eta' \to e^+e^-\gamma$ have been performed by the BESIII collaboration with insufficient statistical precision, therefore the proper theoretical description cannot be determined.

From previous CLAS analyses using the g12 data set, it was preliminarily shown that measurements of the time-like transition form factor were achievable, but without the statistical precision needed to be competitive. Therefore, we propose to use CLAS12 to focus

*Contact person, email: m.kunkel@fz-juelich.de
†Spokesperson

on the dilepton decay channels from the reactions $ep \to e'p\eta'$ and $ep \to e'p\phi$, where $\eta' \to e^+e^-\gamma$ and $\phi \to \eta e^+e^-$. The CLAS12 detector will be used to identify and measure the e^+e^- decay products by means of the High Threshold Cherenkov Counter (HTCC), Pre-Calorimeter (PCAL) and Electromagnetic Calorimeter (EC). The combination of HTCC+PCAL+EC can provide a rejection factor for single $e^\pm/\pi^\pm$ of up to 10^5 for momenta less than 4.9 GeV/c with $\approx 100\%$ efficiency. For dileptons (e^+e^- pairs), this rejection factor will be $\approx 10^{10}$, which enables dilepton studies for branching ratios $\approx 10^{-7}$. Precise determination of momenta and angles of the e^+e^- decay products are the key features available to CLAS12. The momentum and angle of final state photons will be determined in CLAS12 by using the PCAL and EC. Consequently, the photon in the process $\eta' \to e^+e^-\gamma$ and the photons in the process $\phi \to e^+e^-\eta \to e^+e^-\gamma\gamma$ will be detected. Preliminary studies using the CLAS12 simulation suite have shown that a beam time of 100 days, at full luminosity, will accumulate a data sample at least one order of magnitude larger in statistics than the most current $\eta' \to e^+e^-\gamma$ and $\phi \to \eta e^+e^-$ measurement.

Contents

1 Introduction

1.1 Motivation

While very successful in many aspects, the Standard Model of particle physics (SM) leaves a couple of important questions unanswered. On the one hand, it predicts an amount of matter that survived annihilation after the Big Bang that is many orders of magnitude less compared to what is observed. In addition, since masses of matter particles appear as parameters in the SM, it does not provide any understanding why the values of these masses span so many orders of magnitude. In addition, within the SM phenomena like Dark Matter and Dark Energy can not be explained. These and some more issues suggest that there must be physics beyond the SM, and many experiments world-wide hunt for signals of it.

One of the currently most promising candidates to provide a signal for physics beyond the SM is the muon anomaly $a_\mu = (g-2)/2$. It is a low-energy observable, which can be both measured and computed to high precision [1, 2]. The present experimental value $a_\mu^{EXP} = 1\,165\,920\,89(63) \times 10^{-11}$ comes from the BNL E821 experiment [3]. This value deviates from the SM prediction by about 3 standard deviations $\Delta a_\mu^{(\mathrm{EXP-SM})} = (287 \pm 80) \times 10^{-11}$ [4] or $= (261 \pm 78) \times 10^{-11}$ [5], depending on how the leading-order hadronic contributions are evaluated. While this discrepancy is not large enough to claim a failure of the SM, it is currently the largest deviation of a SM prediction from an experimental observable. This alone justifies all efforts currently taken to improve both the theoretical as well as the experimental value. New measurements are planned within the next four years at Fermilab/USA [6] and also at JPARC/Japan [7]. The goal of the measurements is to reduce the uncertainty by a factor of four. In parallel the SM prediction needs to be improved in accuracy by at least a factor of two to establish a deviation from the SM for the first time.

The largest uncertainty of the SM prediction comes from the hadronic quantum corrections [1]. At the level of accuracy that is relevant at the moment the hadronic contributions can be split up into the hadronic vacuum polarization (HVP), displayed on the left-hand side of figure 1, and the hadronic light-by-light scattering (HLbL), displayed in the middle of Fig. 1. The most important contribution to the latter comes from the pseudoscalar

pole contributions, displayed explicitly on the right-hand side of Fig. 1. For those one expects that the contribution should be largely saturated by the lightest exchange particles, namely the π^0, the η and the η'.

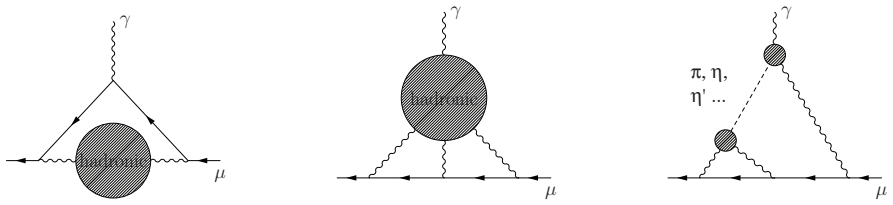

Figure 1: Hadronic contributions to a_μ: hadronic vacuum polarization (left diagram), hadronic light-by-light scattering (middle), pion-pole contribution to hadronic light-by-light scattering (right). Full lines with an arrow denote muons, wiggly lines photons, the dashed line a pseudo-scalar meson and shaded blobs a non-pointlike hadronic substructure.

Concerning the SM prediction for a_μ HLbL is suppressed relative to HVP by one power of the electromagnetic fine structure constant [1, 8]. Unfortunately at present it is not possible to straightforwardly calculate the contributions shown in Fig. 1 from first principles analogously to, e.g., the QED corrections, since both processes concern low-energy corrections, i.e. non-perturbative physics. Thus the prime candidate for a SM calculation of hadronic corrections seems to be lattice QCD [9]. However, it is not expected that lattice QCD results for HPV will reach the required accuracy in the foreseeable future. For the HLbL only preliminary lattice-QCD calculations have been reported [10]. In view of the challenges to determine a four-point function that includes in addition disconnected diagrams it is not clear yet when a profound lattice calculation with controlled uncertainties and a reliable error estimate will be available.

Fortunately there is an alternative way to quantify hadronic corrections. It requires both theoretical as well as experimental efforts: Dispersion theory provides a link between particular hadronic cross sections and a_μ—for a discussion of the HVP in this context see Ref. [1], while for HLbL we refer to Refs. [11, 12, 13, 14]. In particular for the latter contribution it allows one to calculate from the transition form factors of the kind π^0, η, $\eta' \to \gamma^*\gamma^*$ the corresponding piece for the meson pole contribution as displayed in the right most diagram of Fig. 1. The measurements proposed here provide important information towards the necessary input needed for the evaluation of the HLbL contribution, since $\eta' \to \gamma^*\gamma$ gives the single off-shell form factor of the η' and $\phi \to \eta\gamma$ additionally provides information on the isoscalar piece of $\eta \to \gamma^*\gamma$ in a different kinematic regime. Additional information on the η and η' form factors can be found from the dispersive methods outlined in Refs. [15, 16, 17, 18, 19]. It appears to be realistic that this joined effort of

theory and experiment will provide the improvements necessary to push the SM calculation towards the required accuracy.

1.2 History

In the year 1951, Richard Dalitz published a letter [20] in which he calculated the rate for the π^0 decaying into an electron-positron pair (dilepton) and a photon, $\pi^0 \to e^+e^-\gamma$. The calculation assumed that the decay proceeded through a two–photon decay in which one of the photons was virtual and converted internally into an electron-positron pair. This kind of reaction is now known as a Dalitz decay. The experimental evidence of this decay process was first observed in emulsion plates exposed to the Chicago cyclotron in 1952 [21] and a number of experiments performed over the next ten years verified Dalitz's hypothesis that the $\pi^0 \to e^+e^-\gamma$decay resulted from internal conversion of a virtual photon [22, 23, 24]. A few years later N. Kroll and W. Wada calculated the framework for Dalitz decays within the QED framework [25], and extended the framework to double Dalitz Decays, in which the π^0 decays into two electron-positron pairs via emission of two virtual photons. Throughout the following years, much work was done to extend the framework of Dalitz decays to heavier mesons, such as η, ω, η', and ϕ. With numerous experimental data taken, it was shown that the shape of the dilepton mass spectrum deviated from the QED predictions. Such deviations are attributed to the meson not being point-like, as calculated in QED, but instead to the internal structure of the meson. The virtual photon, that decayed into a dilepton pair, has the ability to probe the structure of meson because, like its on-shell counterpart, emission of a virtual photon is radiation, which decouples from any strong interaction within the meson when the meson transitions into its decay. Therefore, the information of the transition is encoded into the virtual photon, known as the Transition Form Factor (TFF), and can be characterized as $\left|F(q^2)\right|$, where q^2 is the square of the invariant mass of the lepton pair. The transition form factor can be determined by comparing QED predictions to the experimentally measured rate.

1.3 Proposal

In this proposal we present an experiment to study two channels of which decay via Dalitz decays, $\eta \to e^+e^-\gamma$ and $\phi \to e^+e^-\eta$. The η and ϕ are produced via electro-production, $ep \to ep\eta'$ and $ep \to ep\phi$ in Hall B, using the CLAS12 detector. The superior $e^+e^-/\pi^+\pi^-$ discrimination of the CLAS12 detector will give access to measurements for which $e^+e^-/\pi^+\pi^-$ branching ratios of 10^{12} is achievable. This proposal is organized as follows. In Section **??** we summarize the current knowledge of Dalitz decays and transition form factors, challenges in dilepton signal quality and how the

CLAS12 detector can surpass the current challenges in measuring a TFF of low statistical error. In Section 2, an explanation of the kinematics of the decay processes will be given as well as kinematics of main competing backgrounds. In Section 3 a brief discussion on past CLAS analysis will be given, along with a description of analysis techniques that have been used and will be used in a CLAS12 measurement. Also in Section 3, an explanation of the Monte-Carlo simulations that were performed to extract the acceptances will be given as well as a calculation of expected yield and a validity check on the expected yield from previous CLAS analyses. In Section **??** we present the beam time request and a summary of the experiment.

2 Kinematics

The two channels proposed to be studied are

$$e(k) + p(p) \rightarrow e'(k') + p'(p') + \eta'(\nu) \tag{1}$$
$$e(k) + p(p) \rightarrow e'(k') + p'(p') + \phi(\nu) \ , \tag{2}$$

where k, k', p, p' are the four–momenta of the incident lepton, outgoing lepton,target proton and scattered proton respectively. The virtual photon in the production is defined as $q = k - k'$ with energy $v = \frac{pq}{m_p} = E - E'$. The quantities $\eta'(\nu)$ and $\phi(\nu)$ are the electro-produced mesons. The production mechanisms of such mesons have been already proposed in previous proposals [26, 27] and are scheduled to run in conjunction with RunGroupA, the same run group requested for in this proposal. The main decays studied for this proposal are:

$$\eta' \rightarrow \gamma\gamma \rightarrow e^+e^-\gamma \tag{3}$$
$$\eta' \rightarrow \gamma\gamma^\star \rightarrow \gamma e^+e^- \tag{4}$$

i.e. when a pseudoscalar meson, $P_p(\eta')$, decays via two photons (Eq. 3) and one photon converts into an e^+e^- pair due to E.M. processes through matter, this is conventionally known as external conversions. This decay channel will he the main background contribution and in further discussed in SecXXX. The Dalitz decay, or internal conversion, is when the $P_p(\eta')$ decays via a real photon and a virtual photon (Eq. 4), which decays into an e^+e^- pair.

$$\phi \rightarrow \eta\gamma \rightarrow \eta e^+e^- \tag{5}$$
$$\phi \rightarrow \eta\gamma^\star \rightarrow \eta e^+e^- \ , \tag{6}$$

i.e. when a vector meson $V_p(\phi)$, decays via an η and a photon(Eq. 5) and one photon converts into an e^+e^- pair. The Dalitz decay for the ϕ is when $V_p(\phi)$ decays via an η and a virtual photon (Eq. 6), which decays into an e^+e^- pair. Figure 2 illustrates the Feynman diagrams for the pseudoscalar

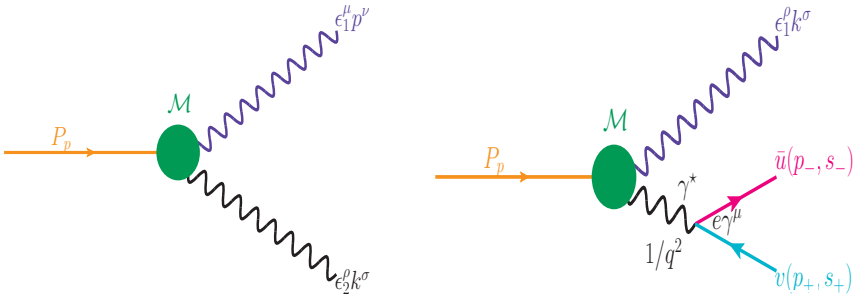

Figure 2: Feynman diagram of $P_p(\eta')$ two photon decay (a), ϵ_1 and ϵ_2 are the polarizations, p and k are 4-momenta of the photons. Feynman diagram of $P_p(\eta')$ Dalitz decay (b), the variable $s_\pm$ are the spin helicities of the outgoing leptons $l^\pm$ with 4-momenta $p_\pm$ and ϵ is the polarization of the outgoing photon with 4-momenta k. In both diagrams $\mathcal{M}$ is the form factor.

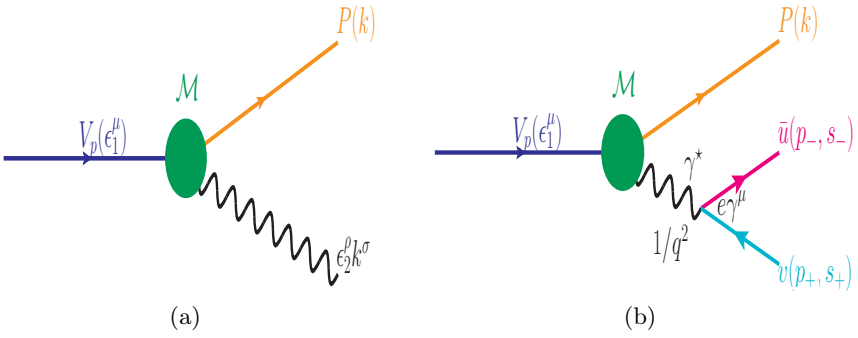

Figure 3: Feynman diagram of $V_p(\phi)$ deacys. Notation same as in Fig. 2.

"two photon decay" and "Dalitz decay", while Fig. 3 illustrates the Feynman diagrams for the vector "pseudoscalar photon decay" and "Dalitz decay". A full derivation of the external conversion and Dalitz decay are given in the Appendix A.

2.1 The Dalitz Decay

The Dalitz decay of mesons is dependent on the spin of the meson. For pseudoscalar meson the decay rate is derived in A.3 and is expressed as:

$$\frac{d\Gamma_{e^+e^-\gamma}}{\Gamma_{\gamma\gamma}dq^2} = \frac{2\alpha}{3\pi}\frac{1}{q^2}\left(1-\frac{q^2}{m_p^2}\right)^3\left(1+\frac{2m_l^2}{q^2}\right)\left(1-\frac{4m_l^2}{q^2}\right)^{\frac{1}{2}} \tag{7}$$

which is the Kroll-Wada equation founded in [25, 28]. For vector mesons, the decay rate can be expressed as:

$$\frac{d\Gamma}{\Gamma_{\eta\gamma}dq^2} = \frac{\alpha}{3\pi}\frac{1}{q^2}\left(\left(1+\frac{q^2}{m_\phi^2-m_\eta^2}\right)^2 - \frac{4m_\phi^2 q^2}{m_\phi^2-m_\eta^2}\right)^{\frac{3}{2}}\left(1+\frac{2m_l^2}{q^2}\right)\left(1-\frac{4m_l^2}{q^2}\right)^{\frac{1}{2}} , \tag{8}$$

as derived as [28]: An example of QED expectation for η' and ϕ is shown in Fig. 4.

2.2 Form Factor

It has been experimentally observed that the shape of the dilepton mass spectrum deviates significantly from the QED predictions, displaying a rise at larger dilepton mass. Therefore, the form factor $M_P(p^2, k^2 = 0)$ or $M_P(p_1^2, p_2^2)$ can be written as follows:

$$M_P \to M_P' \times \left|F(q^2)\right| , \tag{9}$$

where M_P' is the decay constant of two photons or η photon (as mentioned in Sec. A.1), while $\left|F(q^2)\right|$ is called the transition form factor, which defines the electromagnetic space structure of the meson. According to that, the $\eta' \to e^+e^-\gamma$ the decay rate modifies as;

$$\frac{d\Gamma_{e^+e^-\gamma}}{\Gamma_{\gamma\gamma}dq^2} = \frac{2\alpha}{3\pi}\frac{1}{q^2}\left(1-\frac{q^2}{m_p^2}\right)^3\left(1+\frac{2m_l^2}{q^2}\right)\left(1-\frac{4m_l^2}{q^2}\right)^{\frac{1}{2}}\left|F(q^2)\right|^2 , \tag{10}$$

while the $\phi \to \eta e^+e^-$ decay rate modifies as;

$$\frac{d\Gamma_{\eta e^+e^-}}{\Gamma_{\eta\gamma}dq^2} = \frac{\alpha}{3\pi}\frac{1}{q^2}\left(\left(1+\frac{q^2}{m_\phi^2-m_\eta^2}\right)^2 - \frac{4m_\phi^2 q^2}{m_\phi^2-m_\eta^2}\right)^{\frac{3}{2}}\left(1+\frac{2m_l^2}{q^2}\right)\left(1-\frac{4m_l^2}{q^2}\right)^{\frac{1}{2}}\left|F(q^2)\right|^2 , \tag{11}$$

First observations were described with standard vector meson dominance (VMD) where the virtual photon can stem from a intermediate vector mesons. The value of $\left|F(q^2)\right|$ can be directly measured by comparing QED predictions to the measured rate [28].

$$\frac{d\Gamma(A \to B + l^+l^-)}{dq^2\Gamma(A \to B\gamma)} = \left[\frac{d\Gamma}{dq^2}\right]_{\text{QED}} \cdot \left|F(q^2)\right|^2 \tag{12}$$

or by performing a line shape analysis on the l^+l^- invariant mass using assumptions on the structure of $\left|F(q^2)\right|$. One such assumption for $\left|F(q^2)\right|$ is

the dipole approximation from the VMD model, which can be parametrized as:

$$F(q^2) = \frac{1}{1 - q^2/\Lambda^2} \tag{13}$$

where the parameter Λ corresponds to the mass for the effective contributing vector meson.

The slope of the transition form factor, b, is defined as:

$$b \equiv \frac{dF}{dq^2}|_{q^2=0}. \tag{14}$$

and characterizes the intrinsic spatial charge radius for the η' meson, and the $\phi \to \eta$ transition for the ϕ meson.

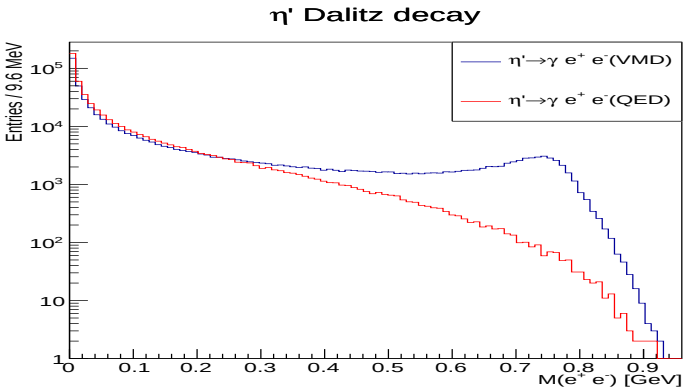

(a)

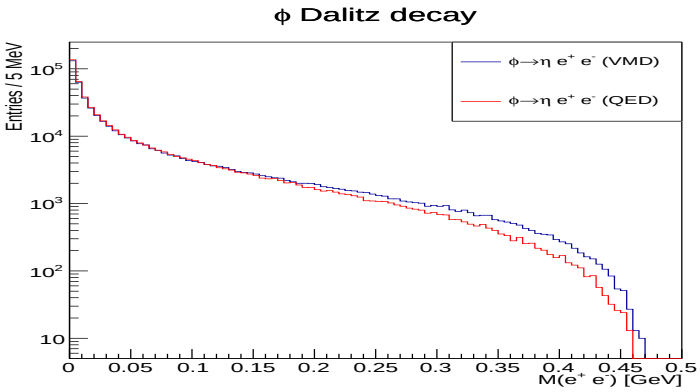

(b)

Figure 4: Example of Dalitz spectra for η' using only QED(red) and the deviation from QED using the VMD parameterization(blue) with 500K Dalitz events generated (a). Example of Dalitz spectra for ϕ using only QED(red) and the deviation from QED using the VMD parameterization(blue) with 500K Dalitz events generated (b).

2.3 Photon Conversion to e^+e^-Pairs

When a photon travels through matter at energies greater than 100 MeV, it can convert into an electron-positron pair. The process of pair production, $\gamma Z \rightarrow Ze^+e^-$, occurs when a photon with $E_0 > 2m_ec^2$ converts into an electron and a positron. The cross section for this process can be written as;

$$\sigma_{\gamma\rightarrow e^+e^-} = \frac{A}{N_A\rho\lambda_\gamma} \ , \ \lambda_\gamma = \frac{9}{7}X_0 \tag{15}$$

where λ is the interaction length, or mean free path, ρ is the density of the material, N_A is Avogadro's number and A is the atomic mass of the

material. The probability of pair production to occur is solely based on X_0, the radiation length of the medium and this probability can be expressed as;

$$\frac{dP}{dx} = \frac{1}{\lambda_\gamma} \exp(\frac{-x}{\lambda_\gamma}) \ . \tag{16}$$

Using the ratio, $\frac{\Gamma_{\eta' \to e^+e^-\gamma}}{\Gamma_{\eta' \to \gamma\gamma}} = 2.13 \cdot 10^{-2}$, that has been preliminary measured by CLAS, which is consistent with [29], the probability of pair production when a photon, from the $\eta' \to \gamma\gamma$ decay, traveling though 5 cm of liquid hydrogen, ℓH_2, is shown in Fig. 5 as well as the number of $\eta' \to \gamma\gamma \to e^+e^-\gamma$ / $100\eta' \to e^+e^-\gamma$. Since CLAS12 has a vertex resolution of ≈1 mm the

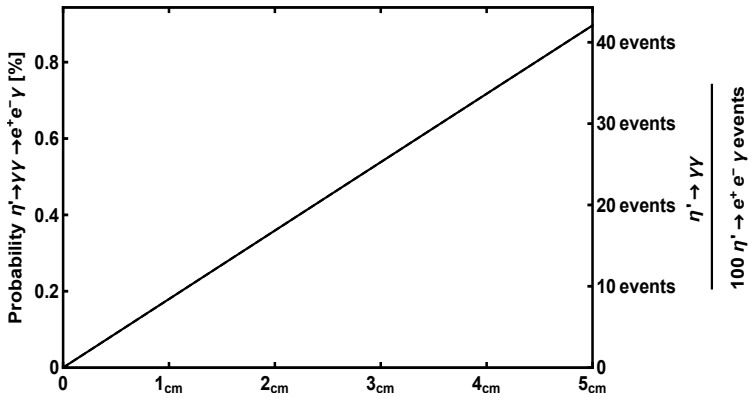

Figure 5: (Left axis)Probability of pair production, $\gamma \to e^+e^-$; (Right axis) number of $\eta' \to \gamma\gamma \to e^+e^-\gamma$ / $100\eta' \to e^+e^-\gamma$ as a function of distance in liquid hydrogen.

probability of pair production traveling through 10 mm is shown in Fig. 6. Therefore, a 1 mm cut on the primary vertex will yield a contamination of ≈ one externally converted $e^+e^-$from $\eta' \to \gamma\gamma \to e^+e^-\gamma$ per Dalitz decays $100\eta' \to e^+e^-\gamma$ These type of subprocess mimics the Dalitz decay $\eta' \to e^+e^-\gamma$, described in Sec. A.3. Since there are two photons with equal probability of conversion for $\eta' \to \gamma\gamma$, the total probabilities shown is for when either photon externally converts. Using the ratio, $\frac{\Gamma_{\phi \to e^+e^-\eta}}{\Gamma_{\phi \to \gamma\eta}} = 9.58 \cdot 10^{-2}$ [30], the probability of pair production when a photon, from the $\phi \to \gamma\eta$ decay, traveling though 5 cm of liquid hydrogen, ℓH_2, is shown in Fig. 7 as well as the number of $\phi \to \gamma\eta \to e^+e^-\eta$ / $100\phi \to e^+e^-\eta$. Since CLAS12 has a vertex resolution of ≈1 mm the probability of pair production traveling through 10 mm is shown in Fig. 6. Therefore, a 1 mm cut on the primary vertex will yield a contamination of ≈ one externally converted $e^+e^-$from $\phi \to \gamma\eta \to e^+e^-\eta$ per Dalitz decays $100\phi \to e^+e^-\eta$ From multiple scattering effects the e^+e^- from a converted photon will obtain a mass distribution. Simulations of photons from η' and ϕ radiative decays traversing

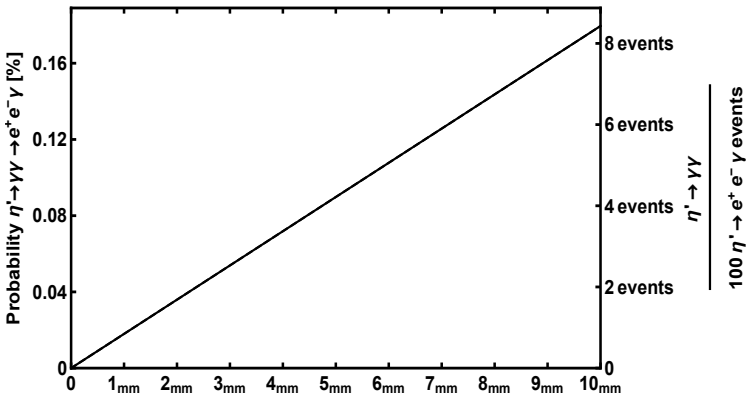

Figure 6: (Left axis)Probability of pair production, $\gamma \rightarrow e^+e^-$; (Right axis) number of $\eta' \rightarrow \gamma\gamma \rightarrow e^+e^-\gamma$ / $100\eta' \rightarrow e^+e^-\gamma$ as a function of distance in liquid hydrogen.

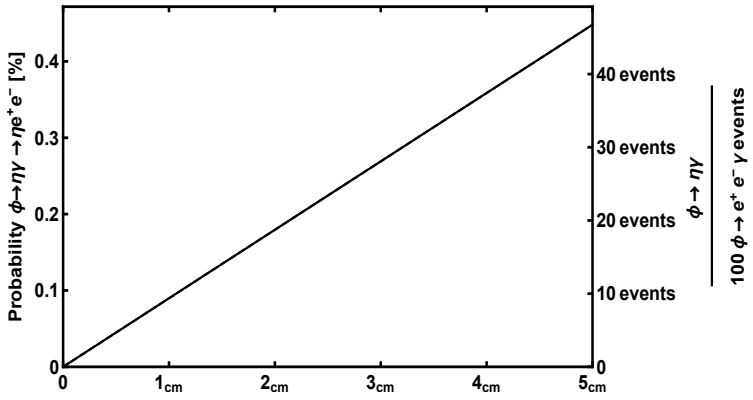

Figure 7: (Left axis)Probability of pair production, $\gamma \rightarrow e^+e^-$; (Right axis) number of $\phi \rightarrow \gamma\eta \rightarrow e^+e^-\eta$ / $100\phi \rightarrow e^+e^-\eta$ as a function of distance in liquid hydrogen.

through 1 mm of ℓH_2 show that the e^+e^-can obtain a maximum mass of ~ 0.14 GeV.

2.4 Summary

The $\gamma\gamma$ decay and the $\gamma^\star\gamma$ decay have different branching ratios as do the decays $\gamma\eta$ decay and the $\gamma^\star\eta$. This difference is attributed to the factor of α along with a q^2 dependence calculated in the Dalitz decay. However, due to the probability of a photon converting into an electron-positron pair in $\ell\mathrm{H}_2$, the total amount of e^+e^-pairs produced via photon conversion can

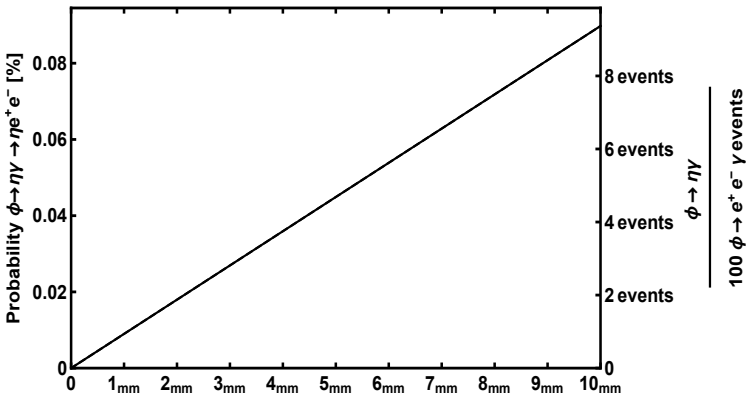

Figure 8: (Left axis)Probability of pair production, $\gamma \to e^+e^-$; (Right axis) number of $\phi \to \gamma\eta \to e^+e^-\eta$ / $100\phi \to e^+e^-\eta$ as a function of distance in liquid hydrogen.

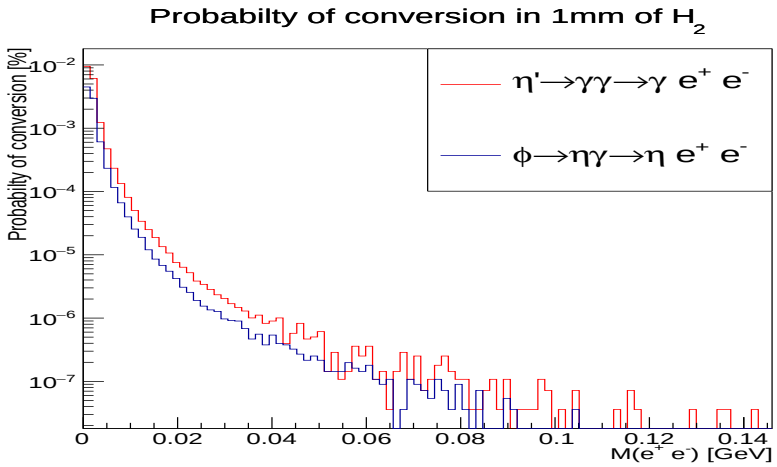

Figure 9: Probability of pair production in 1 mm of ℓH_2 for $\eta' \to \gamma\gamma$ and $\phi \to \gamma\eta$ vs. $M(e^+e^-)$

contaminate the measurement of the form factor. The CLAS detector will have vertex resolution of ∼1 mm, therefore the amount of contamination of externally converted pairs will be minimized by the vertex position of the e^+e^-pair. An example of the total contamination, in the Dalitz spectrum, from external conversion within 1 mm of the primary vertex can be seen in Fig. 10.

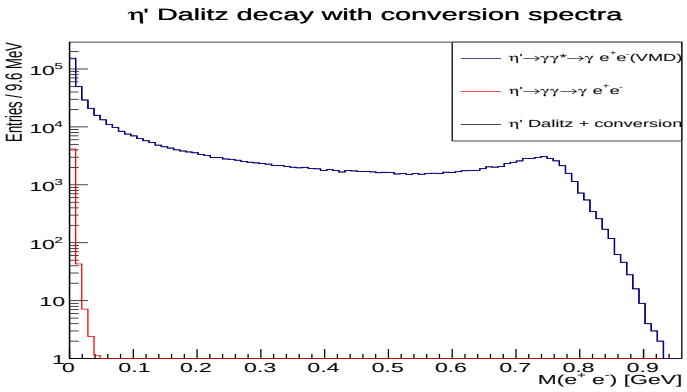

(a)

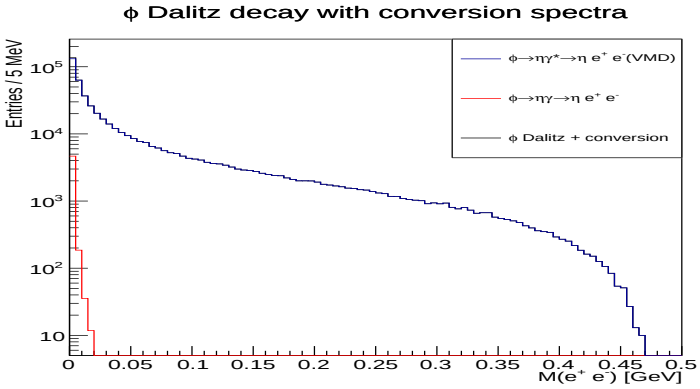

(b)

Figure 10: Example of Dalitz and conversion spectra for η' with 500K Dalitz events generated and $\sim 2.35 \cdot 10^7$ $\eta' \to \gamma\gamma$ generated (a). Example of Dalitz and conversion spectra for ϕ with 500K Dalitz events generated and $\sim 5.7 \cdot 10^7$ $\phi \to \eta\gamma$ generated (b).

3 Measurement

This section will describe the previous published results on transition form factors as well as current CLAS analyses. A summary on the CLAS preliminary result on the η' with the emphasize on the desire to further this measurement in CLAS12. Also in this section is a description on how the $\eta \to e^+e^-\gamma$ and $\phi \to e^+e^-\eta$ were simulated and reconstructed for this CLAS12 proposal.

3.1 Current Experimental Results

Several experimental groups are currently investigating decays of light mesons, including the

- TRIUMF $\pi^0 \to e^+e^-\gamma$ [31] (Transition form factor)
- A2 Collaboration $\eta \to e^+e^-\gamma$ [32, 33] (Transition form factor)
- Multiple Groups $\omega \to \pi^0\mu^+\mu^-$ [36, 37, 38](Transition form factor)
- BESIII Collaboration $\eta' \to e^+e^-\gamma$ [34] (Transition form factor)
- KLOE Collaboration $\phi \to e^+e^-\eta$ [35] (Transition form factor)

The experiential results of the π^0 and ω present a puzzle because for the π^0 the measurement in the time-like region does not have agreement between several experiemtn

The experimental results on the conversion decay of the ω meson, $\omega \to \pi^0\mu^+\mu^-$ present a puzzle [36, 37, 38]. The measurements suggest a dramatic increase of the transition form factor for large momentum transfers that is not consistent with VMD models nor explicable with modern theoretical advances. These experimental results are in contradiction to measurements in the space-like regime [39]. The situation makes it important to investigate the conversion decays of vector mesons.

... mention A2 measurement ? ...

The conversion decays of the ω meson are currently being studied within the LMD group using data from the CLAS g12 experiment. We plan to approach the conversion decays of the ϕ meson by analyzing the decay $\phi \to \eta\gamma^\star$ based on the proposed experiment. The decay $\phi \to \pi^0\gamma^\star$ would enable access to higher dilepton masses and more precise mapping of transition form factors in this kinematic regime. However, the decay is OZI suppressed and statistically significant results may be obtained after a luminosity upgrade of the experiment facility. Current measurements by the KLOE collaboration for $\phi \to \eta e^+e^-$ [35] and $\phi \to \pi^0 e^+e^-$ [40] have improved the values for the respective branching ratios by the SND and CMD-2 collaborations [41, **?**, 42, 43]. The $\phi \to \eta e^+e^-$ measurement by KLOE is based on 31000 events and deduces a slope parameter of KLOE $b_{\phi\eta} = 1.28 \pm 0.10^{+0.09}_{-0.08}$.

... figure of KLOE phi-eta TFF here? ...

3.2 Previous CLAS analyses

LMD (Light Meson Decay) group of CLAS. The g12 experiment performed at CLAS produced data set of photon-induced reactions. Fortunately, the Cherenkov Counters(CC) were filled with perflourbutane (C_4F_{10}) and a trigger consisting of a coincidence between the (ST·TOF)(CC·EC) allowing the study of dilepton reactions throughout the entire beam energy range

1.15 GeV $< E_\gamma <$ 5.45 GeV. Preliminary analyses of g12 involving dileptons include the decays:

- $\Delta \to pe^+e^-$ (Transition form factor)
- $\eta \to e^+e^-\gamma$ (Transition form factor)

while advanced analyses involving dileptons include:

- $\pi^0 \to e^+e^-\gamma$ (Differential Cross-Section)
- $\omega/\rho \to e^+e^-$ (Interference of ω/ρ)
- $\omega \to e^+e^-\pi^0$ (Transition form factor)
- $\eta' \to e^+e^-\gamma$ (Transition form factor / branching ratio)

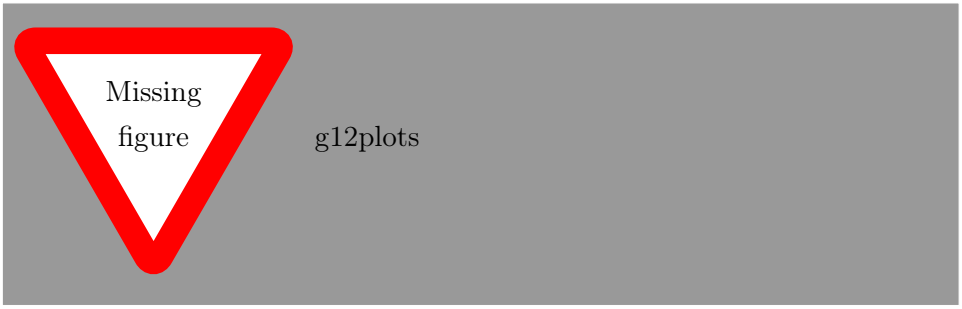

As seen in Fig. the current CLAS results suffer from insufficient statistics. Therefore, we propose to repeat the $\eta' \to e^+e^-\gamma$ measurement with CLAS12.

3.3 Simulation and Reconstruction

To simulate the reactions in Eq. 1 and Eq. 2, the program PLUTO++ [44] was utilize for its ability to simulate the decays of those according to QED, Vector Meson Dominance or a user inputted TFF. For reconstruction of the desired topologies, the CLAS12 FASTMC [45] was used, in which $\sim 9 \cdot 10^6$ events were generated for $\eta' \to e^+e^-\gamma$ and $\phi \to e^+e^-\eta$ and then simulated with FASTMC at 75% torus field. An extra simulation was performed for the torus field setting of 100% to show the effects of the magnetic field on the lepton acceptance. All detector efficiencies are assumed to be 100% except the EC efficiency, in which an efficiency of 10% was factored for each detected lepton. This EC efficiency was calculated with the g12 data set and the assumption is that the CLAS12 EC efficiency will be at least the same as the previous CLAS EC since the EC is the same sub-detector in both detectors.

The production of each particle was weighted by photo-production differential cross-sections, $\frac{d\sigma}{d\Omega}(v, \cos\theta_{cm})$, published in [46], where v is the virtual photon energy. This was done to achieve a quasi realistic model of the

production. The e^+e^- decay spectrum, of each meson, was weighted via the VMD model (including QED predictions). Another simulation was performed using a flat $M(e^+e^-)$ distribution (No QED, No VMD) to analyze any effects of the model on the e^+e^-acceptance. The analysis showed that this acceptance was independent of the decay model, see Fig.13 and Fig.14.

3.3.1 Trigger Requirements

The standard CLAS12 electron trigger (HTCC(Nphe>2) * [(PCAL+EC)>1.0 GeV] is sufficient for these types of analyses. It has been shown in previous proposals [47, 48] that the rate of the standard electron trigger will be 6 kHz, which the expected data acquisition (DAQ) readout rate is 10 kHz.

3.3.2 Detection of e^+e^-Events

Electron/positron ID will include responses from the HTCC, PCAL and EC calorimeters. The energy information of the PCAL and the inner and outer parts of EC will be used to compare the total energy deposition with the momentum measured in the DC ($\alpha * (\mathrm{E_{Pcal}} + \mathrm{E_{ECin}} + \mathrm{E_{ECout}}) \sim \mathrm{P_{DC}}$), where α is a scaling factor.

3.3.3 Particle Identification

The η' and ϕ mesons have pion decay modes, which are orders of magnitude greater than the Dalitz decay. For the η' meson, for example, the ratio $\Gamma\pi^+\pi^-\gamma/\Gamma e^+e^-\gamma$ is $6.2 \cdot 10^2$. Electrons/positrons will be identified by using the information from the detectors described above. The expected $e^\pm/\pi^\pm$ rejection factor for single particles (p<4.9 GeV) is 10^3 for the HTCC, while the PCAL+EC can provide an additional factor of 10^2. Combining both methods yields a $e^\pm/\pi^\pm$ rejection factor of 10^5 which results in a $e^+e^-/\pi^+\pi^-$ rejection factor of 10^{10}. Therefore, the amount of $\pi^+\pi^-$ background in the $M(e^+e^-)$ spectrum will be $\approx 6.2 \cdot 10^2/10^{10} = 6.2 \cdot 10^{-8}$. A detailed explanation of particle identification for e^+e^- pairs can be found in [48].

3.3.4 Acceptance

An exclusive reconstruction scheme

$$ep \to e'p\eta' \to pe^+e^-\gamma \tag{17}$$

$$ep \to e'p\phi \to pe^+e^-\eta\ , \tag{18}$$

where all final state particle are detected, as well as an inclusive reconstruction scheme

$$ep \to e'p\eta' \to e^+e^-\gamma(p) \tag{19}$$

$$\tag{20}$$

where the proton was not detected, was analyzed. Figure 11 and Fig. 12 show the generated e^+e^- spectrum along with the accepted events for both reconstruction schemes. The acceptance was calculated by dividing the accepted events by the generated events, per $M(e^+e^-)$ bin. The η' Dalitz decay acceptance can be seen in Fig.13 and the ϕ Dalitz decay acceptance in Fig..

add reference to plot once done

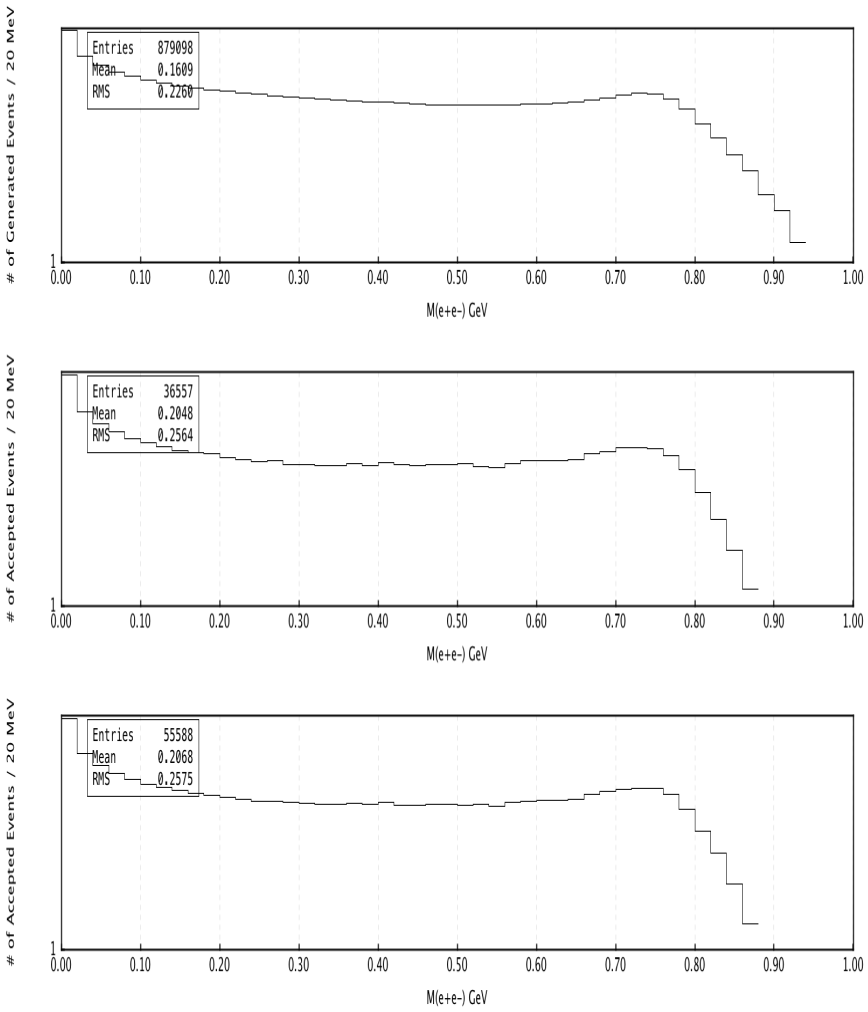

Figure 11: Generated events (Top), accepted events for an exclusive (Middle), inclusive(Bottom) reconstruction schemes as a function of $M(e^+e^-)$. In all panels a VMD decay model was employed

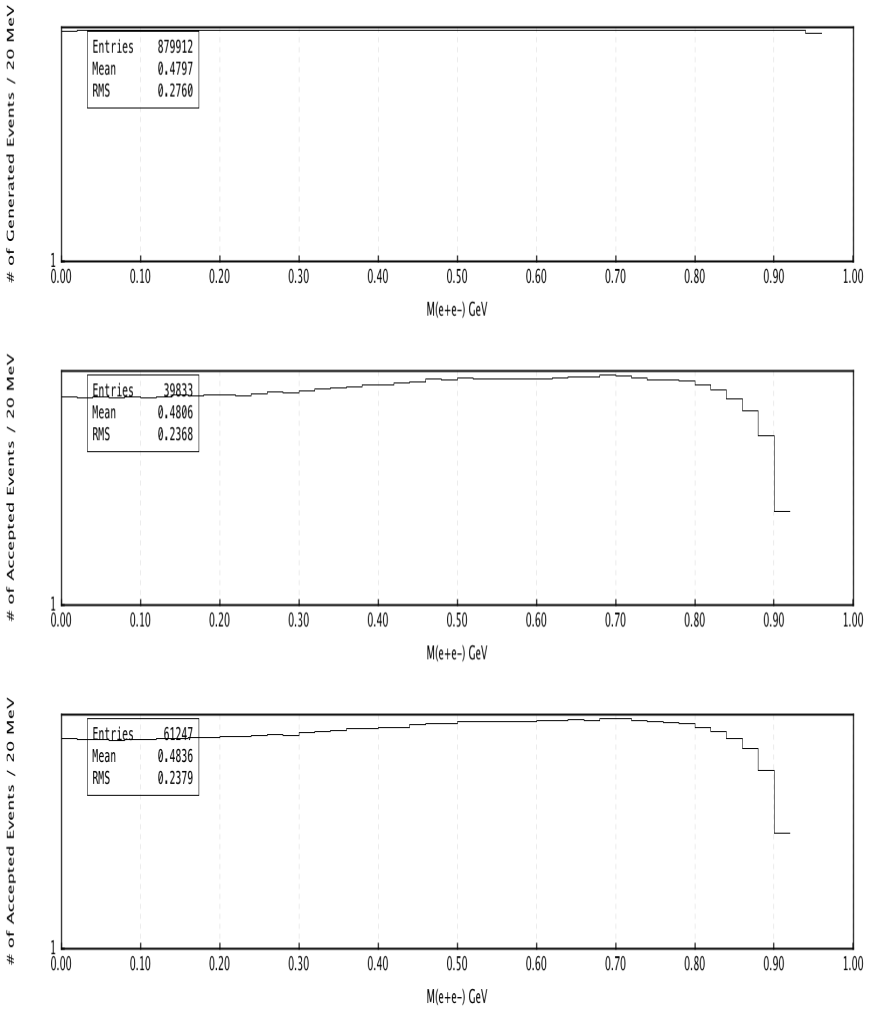

Figure 12: Generated events (Top), accepted events for an exclusive (Middle), inclusive(Bottom) reconstruction schemes as a function of $M(e^+e^-)$. In all panels a Flat e^+e^- decay model was employed

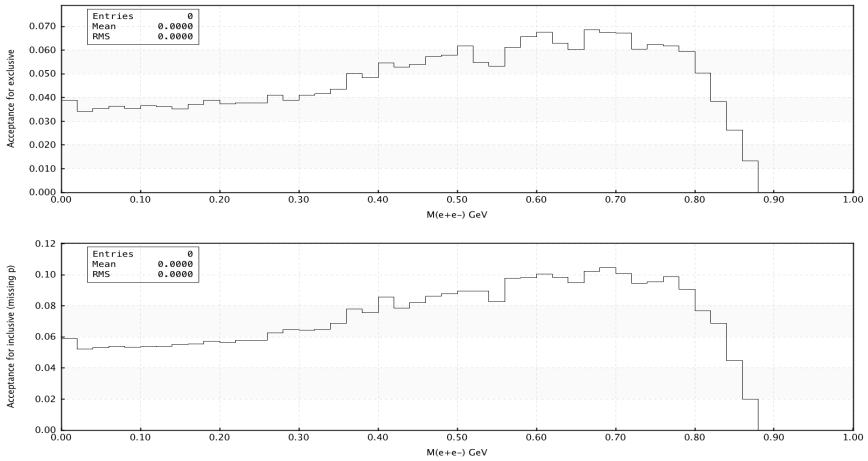

Figure 13: Acceptance using a VMD decay model, as a function of $M(e^+e^-)$ for the exclusive (Top) and inclusive reconstruction scheme(Bottom).

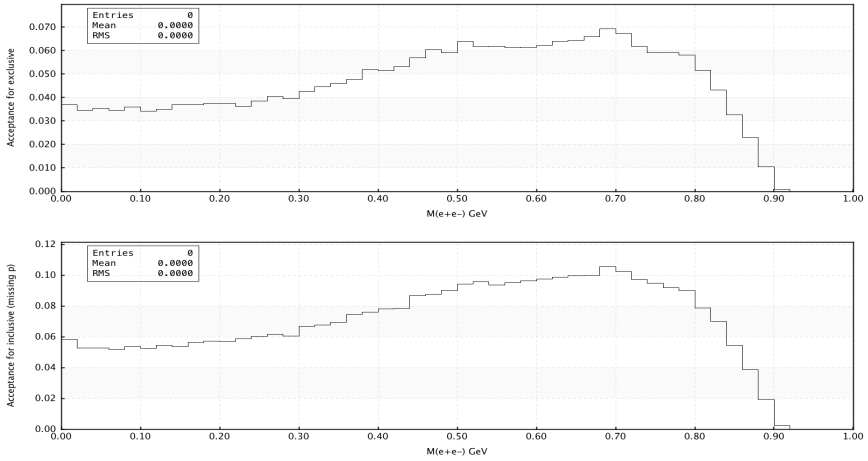

Figure 14: Acceptance using a flat e^+e^- decay model, as a function of $M(e^+e^-)$ for the exclusive (Top) and inclusive reconstruction scheme(Bottom).

3.4 Calculating Expected Yield

3.4.1 Calculating Photon Flux

A simple method for calculating the photon flux in CLAS12 is as follows; Using the fact that g12 had a photon flux of $7 \cdot 10^7$ γ/s on a Au radiator of $10^{-4}\chi_0$ an expected $\sim 4 \cdot 10^9 \gamma$/s will be seen in CLAS12 at $\mathcal{L} = 10^{35}\text{cm}^{-2}\text{s}^{-1}$ on a 5 cm ℓH_2 target which is $\sim 5.7 \cdot 10^{-3}\chi_0$. This number has been independently confirmed in a previous CLAS proposal [47].

3.4.2 Calculating Yield

The average number of meson $\rightarrow e^+e^-X$ expected in CLAS12 can be calculated as:

$$\bar{N}(e^+e^-)_{\text{meson}\rightarrow e^+e^-X} = \Phi\epsilon(e^+e^-)\bar{\sigma}\rho_{\ell_{H_2}}\ell_{target}N_A\frac{\Gamma_{\text{tot}_{\text{meson}}}}{\Gamma_{\text{meson}\rightarrow e^+e^-X}} \ , \qquad (21)$$

where Φ is the photon flux estimated in Sec. 3.4.1, ϵ is the acceptance, $\bar{\sigma}$ is the total cross-section, $\rho_{\ell_{H_2}}$ is the atomic density of ℓ_{H_2}, ℓ_{target} is the target length, N_A is Avogadro's constant, and $\frac{\Gamma_{\text{tot}_{\text{meson}}}}{\Gamma_{\text{meson}\rightarrow e^+e^-X}}$ is the total branching fraction of the meson decaying into e^+e^-X. Using the lepton acceptance shown is Sec. 3.3.4 the average number of η' per $M(e^+e^-)$ can be seen in Fig. 15.

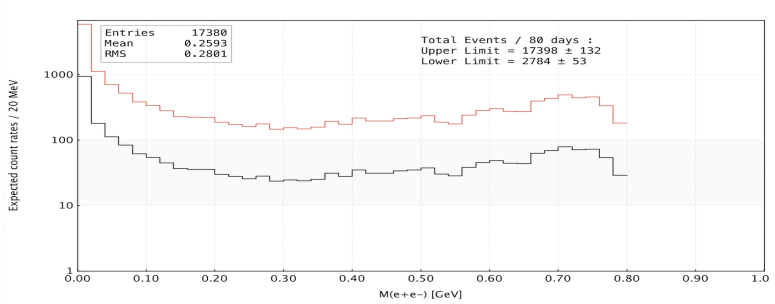

(a)

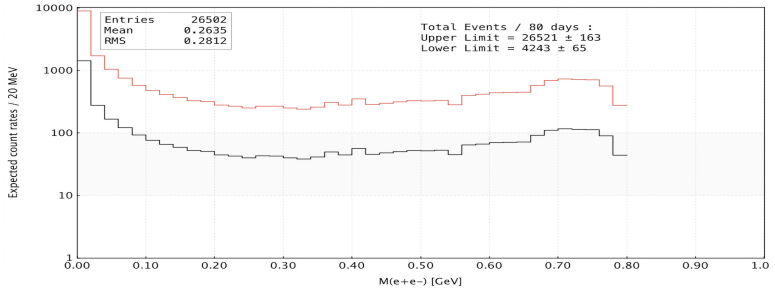

(b)

Figure 15: Count rates for the exclusive (a) and inclusive (b). For both plots the photon detection efficiency was assumed to be between 10%(Red) and 2%(Black).

Integrating over $M(e^+e^-)$, the expected yield calculates to be $17,398$ events for exclusive scheme and $26,521$ events for the inclusive scheme. This would increase the world statistics by a factor of $\sim$ 20 and $\sim$ 30 respectively. Table 1 and Tab. 2 in App. B depicts the upper and lower amount of e^+e^-expected from 80 days of beam time for two torus fields of 75% and 100% respectively.

3.5 Realistic Yield

As a reality check, lets compute the number of $\eta' \to e^+e^-\gamma$ that g12 would have seen, had the experiment ran for 80 days with a real photon flux as calculated for CLAS12 (Sec. 3.4.1). The 89 $\eta' \to e^+e^-\gamma$ events produced in g12 were recorded when the e^+e^-trigger was established. This time was

66% of the total 44 days, which is $\sim$ 29 days. The total integrated flux measured during this time was $\sim 8.8 \cdot 10^{13}$ photons. Therefore, in 80 days the total integrated flux would have been $\sim 2.4 \cdot 10^{14}$ and the total number of $\eta' \to e^+e^-\gamma$ events recorded would have been 242. The ratio of g12 total flux at 80 days per CLAS12 real photon flux is $2.73 \cdot 10^{16}/2.4 \cdot 10^{14} \sim 114$. Therefore g12 would have recorded $114 \cdot 242 = 27590$ $\eta' \to e^+e^-\gamma$ events, which is consistent with what is proposed to be measured with 80days, in the inclusive reconstruction scheme for either torus field setting. See Sec. B for total count rates.

3.6 Acceptance at 100% Torus field

An addition simulation was performed using the same generated data shown above, the difference being the setting of the torus magnetic field. Below, in Fig. 16, the ratio of the lepton acceptance for the two different torus settings is depicted.

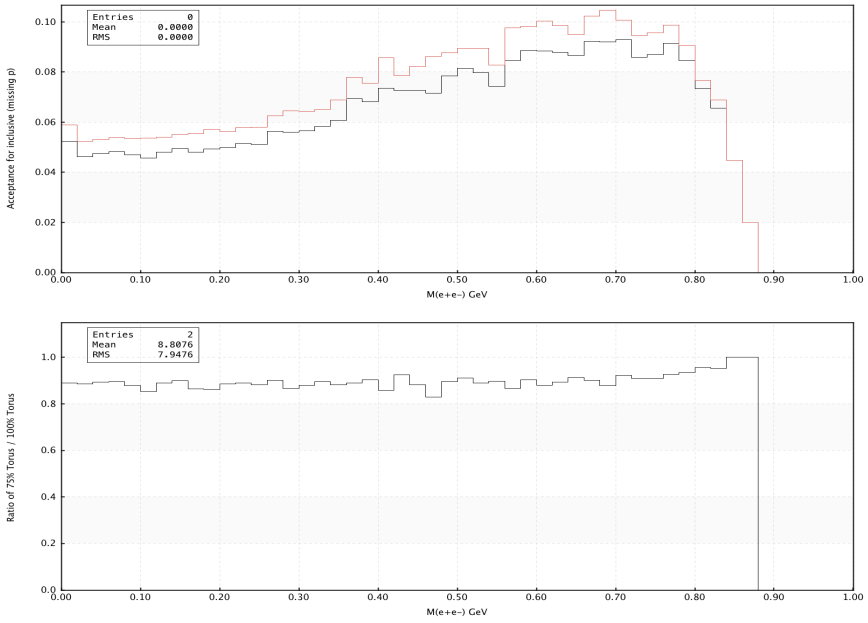

Figure 16: Acceptance using a VMD decay model, as a function of $M(e^+e^-)$ for the inclusive scheme(Top). The torus field was set to 75%(red) as well as 100%(black). Ratio of the acceptances plotted above (75%/100%)(Bottom).

3.7 Expected Systematic Uncertainties

The major sources of systematic uncertainties are the acceptance and particle identification. The lepton acceptance uncertainty is estimated to be $\lesssim$

5% which was observed in former CLAS experiments. The lepton identification uncertainty will arise from the performance of the HTCC, PCAL and EC. From simulation studies performed for this proposal, all leptons and final state photons are detected within the geometric space of the PCAL+EC with hit coincidences in both. Furthermore, all leptons, within a few percent, that were detected in the PCAL+EC were also detected in the HTCC. Further systematics from pion contamination are mitigated by the pion rejection factor described above. Systematics related to external photon conversion are minimal due to the 1 mm resolution of the primary vertex given by the Silicon Vertex Tracker (SVT) as shown in Sec 2.3. Any Bethe-Heitler contributions are negligible when utilizing and exclusive meson reconstruction scheme.

4 Manpower

To analyze the $\eta' \to e^+e^-\gamma$ and $\phi \to e^+e^-\eta$ decays, a minimum of one postdoctoral associate and one graduate student will be needed to perform the following tasks:

or allotted?

- Aide in the calibration of RunGroupA
- Skim and analyze the e^+e^- data
- Simulate and correct the data
- Write publications of the results

5 Beam Time Request

With this proposal and beam time request, we ask for 100 days of beam time. Of the 100 days, 80 days will be dedicated to the production beam time with the standard CLAS setup, at full luminosity ($\sim 10^{35}\text{cm}^{-2}\text{s}^{-1}$) with 75% torus field. The remaining 20 days will be dedicated to optimizing and testing the trigger set-up (HTCC +PCAL + EC). This request should provide a competitive data sample of $\eta' \to e^+e^-\gamma$ and $\phi \to e^+e^-\eta$. The CLAS12 configuration we propose for the measurement of the transition form factors is compatible with the experimental setup already established by Run Group A.

References

[1] Fred Jegerlehner and Andreas Nyffeler. The Muon g-2. *Phys. Rept.*, 477:1–110, 2009.

[2] Thomas Blum, Achim Denig, Ivan Logashenko, Eduardo de Rafael, B. Lee Roberts, Thomas Teubner, and Graziano Venanzoni. The Muon (g-2) Theory Value: Present and Future. 2013.

[3] G. W. Bennett et al. Final Report of the Muon E821 Anomalous Magnetic Moment Measurement at BNL. *Phys. Rev.*, D73:072003, 2006.

[4] Michel Davier, Andreas Hoecker, Bogdan Malaescu, and Zhiqing Zhang. Reevaluation of the Hadronic Contributions to the Muon g-2 and to alpha(MZ). *Eur. Phys. J.*, C71:1515, 2011. [Erratum: Eur. Phys. J.C72,1874(2012)].

[5] Kaoru Hagiwara, Ruofan Liao, Alan D. Martin, Daisuke Nomura, and Thomas Teubner. (g-2)$_m u$ and alpha(M_Z^2) re-evaluated using new precise data. *J. Phys.*, G38:085003, 2011.

[6] J. Grange et al. Muon (g-2) Technical Design Report. 2015.

[7] Naohito Saito. A novel precision measurement of muon g-2 and EDM at J-PARC. *AIP Conf. Proc.*, 1467:45–56, 2012.

[8] Johan Bijnens and Joaquim Prades. The Hadronic Light-by-Light Contribution to the Muon Anomalous Magnetic Moment: Where do we stand? *Mod. Phys. Lett.*, A22:767–782, 2007.

[9] Christof Gattringer and Christian B. Lang. Quantum chromodynamics on the lattice. *Lect. Notes Phys.*, 788:1–343, 2010.

[10] Thomas Blum, Saumitra Chowdhury, Masashi Hayakawa, and Taku Izubuchi. Hadronic light-by-light scattering contribution to the muon anomalous magnetic moment from lattice QCD. *Phys. Rev. Lett.*, 114(1):012001, 2015.

[11] Gilberto Colangelo, Martin Hoferichter, Massimiliano Procura, and Peter Stoffer. Dispersive approach to hadronic light-by-light scattering. *JHEP*, 09:091, 2014.

[12] Vladyslav Pauk and Marc Vanderhaeghen. Anomalous magnetic moment of the muon in a dispersive approach. *Phys. Rev.*, D90(11):113012, 2014.

[13] Gilberto Colangelo, Martin Hoferichter, Bastian Kubis, Massimiliano Procura, and Peter Stoffer. Towards a data-driven analysis of hadronic light-by-light scattering. *Phys. Lett.*, B738:6–12, 2014.

[14] Gilberto Colangelo, Martin Hoferichter, Massimiliano Procura, and Peter Stoffer. Dispersion relation for hadronic light-by-light scattering: theoretical foundations. *JHEP*, 09:074, 2015.

[15] P. Adlarson et al. Exclusive Measurement of the $\eta \to \pi^+\pi^-\gamma$ Decay. *Phys. Lett.*, B707:243–249, 2012.

[16] F. Stollenwerk, C. Hanhart, A. Kupsc, U. G. Meissner, and A. Wirzba. Model-independent approach to eta -> pi+ pi- gamma and eta' -> pi+ pi- gamma. *Phys. Lett.*, B707:184–190, 2012.

[17] C. Hanhart, A. Kup?c, U. G. Meißner, F. Stollenwerk, and A. Wirzba. Dispersive analysis for $\eta \to \gamma\gamma^*$. *Eur. Phys. J.*, C73(12):2668, 2013. [Erratum: Eur. Phys. J.C75,no.6,242(2015)].

[18] Bastian Kubis and Judith Plenter. Anomalous decay and scattering processes of the η meson. *Eur. Phys. J.*, C75(6):283, 2015.

[19] C. W. Xiao, T. Dato, C. Hanhart, B. Kubis, U. G. Meißner, and A. Wirzba. Towards an improved understanding of eta –> gamma* gamma*. 2015.

[20] R H Dalitz. On an alternative decay process for the neutral π^0-meson. *Proceedings of the Physical Society. Section A*, 64(7):667, 1951.

[21] J. J. Lord, Joseph Fainberg, D. M. Haskin, and Marcel Schein. Narrow angle pairs of particles from nuclear interactions. *Phys. Rev.*, 87:538–539, Aug 1952.

[22] N. P. Samios. Dynamics of internally converted electron-positron pairs. *Phys. Rev.*, 121:275–281, Jan 1961.

[23] P. Lindenfeld, A. Sachs, and J. Steinberger. The Internal Pair Production of γ-Rays of Mesonic Origin; Alternate Modes of π^0 Decay. *Physical Review*, 89:531–537, February 1953.

[24] C. P. Sargent, R. Cornelius, M. Rinehart, L. M. Lederman, and K. Rogers. Diffusion cloud-chamber study of very slow mesons. i. internal pair formation. *Phys. Rev.*, 98:1349–1354, Jun 1955.

[25] Norman M. Kroll and Walter Wada. Internal pair production associated with the emission of high-energy gamma rays. *Phys. Rev.*, 98:1355–1359, Jun 1955.

[26] P. Stoler et al. Hard exclusive electroproduction of pi0 and eta with clas12. Technical report, `CLAS` Analysis Proposal `E12-06-108`, 2011.

[27] P. Stoler et al. Exclusive phi meson electroproduction with clas12. Technical report, `CLAS` Analysis Proposal `E12-12-007`, 2012.

[28] L.G. Landsberg. Electromagnetic decays of light mesons. *Physics Reports*, 128(6):301 – 376, 1985.

[29] M. Ablikim and et. al. Observation of the dalitz decay $\eta' \to \gamma e^+ e^-$. *Phys. Rev. D*, 92:012001, Jul 2015.

[30] K.A. Olive et al. Review of particle physics. *Phys. Rev. C*, 38:090001, 2014.

[31] F. Farzanpay et al. Measurement of the slope of the π^0 electromagnetic form factor. *Physics Letters B*, 278(4):413 – 418, 1992.

[32] H. Berghäuser et al. Determination of the η-transition form factor in the reaction. *Physics Letters B*, 701(5):562 – 567, 2011.

[33] P. Aguar-Bartolomé and others. New determination of the η transition form factor in the dalitz decay $\eta' \to e^+ e^- \gamma$ with the crystal ball/taps detectors at the mainz microtron. *Phys. Rev. C*, 89:044608, Apr 2014.

[34] M. Ablikim et al. Observation of the Dalitz Decay $\eta' \to \gamma e^+ e^-$. *Phys. Rev.*, D92(1):012001, 2015.

[35] D. Babusci et al. Study of the Dalitz decay $\phi \to \eta e^+ e^-$ with the KLOE detector. *Phys. Lett.*, B742:1–6, 2015.

[36] R. I. Dzhelyadin et al. Study of the Electromagnetic Transition Formfactor in $\omega \to \pi^0 \mu^+ \mu^-$ Decay. *Phys. Lett.*, B102:296, 1981. [JETP Lett.33,228(1981)].

[37] R. Arnaldi et al. Study of the electromagnetic transition form-factors in eta —> mu+ mu- gamma and omega —> mu+ mu- pi0 decays with NA60. *Phys. Lett.*, B677:260–266, 2009.

[38] Antonio Uras. Measurement of the η and ω Dalitz decays transition form factors in p-A collisions at 400 GeV/c with the NA60 apparatus. *J. Phys. Conf. Ser.*, 270:012038, 2011.

[39] M. N. Achasov et al. Study of $e^+ e^- \to \omega\pi^0 \to \pi^0 \pi^0 \gamma$ in the energy range $1.05 - 2.00$ GeV with SND. *Phys. Rev.*, D88(5):054013, 2013.

[40] A. Anastasi et al. Measurement of the $\phi \to \pi^0 e^+ e^-$ transition form factor with the KLOE detector. *Phys. Lett.*, B757:362–367, 2016.

[41] M. N. Achasov et al. Study of Conversion Decays phi –> eta e+ e- and eta –> gamma e+ e- in the Experiment with SND Detector at the VEPP-2M Collider. *Phys. Lett.*, B504:275–281, 2001.

[42] M. N. Achasov et al. Measurement of the phi –> pi0 e+ e- decay probability. *JETP Lett.*, 75:449–451, 2002. [Pisma Zh. Eksp. Teor. Fiz.75,539(2002)].

[43] R. R. Akhmetshin et al. Observation of the conversion decay phi —> pi0 e+ e- at CMD-2. *Phys. Lett.*, B503:237–244, 2001.

[44] I. Frohlich, I. Froehlich, Lorenzo Cazon, T. Galatyuk, V. Hejny, et al. Pluto: A Monte Carlo Simulation Tool for Hadronic Physics. *PoS*, ACAT2007:076, 2007.

[45] CLAS software repository. Monte-carlo program to simulate clas12 detector response. Technical report.

[46] M. Williams et al. Differential cross sections for the reactions $\gamma p \to p\eta$ and $\gamma p \to p\eta^{'}$. *Phys. Rev. C*, 80:045213, Oct 2009.

[47] M. Battaglieri et al. Meson spectroscopy with low Q2 electron scattering in CLAS12. Technical report, `CLAS` Analysis Proposal `E12-11-005`, 2010.

[48] P. Nadel-Turonski et al. Timelike Compton Scattering and J/ψ photoproduction on the proton in e+e- pair production with CLAS12 at 11 GeV. Technical report, `CLAS` Analysis Proposal `E12-12-001`, 2012.

[49] M.E. Peskin and D.V. Schroeder. *An Introduction to Quantum Field Theory*. Advanced book classics. Addison-Wesley Publishing Company, 1995.

[50] F. Halzen and A.D. Martin. *Quarks and leptons: an introductory course in modern particle physics*. Wiley, 1984.

[51] C. Hanhart, A. Kupść, U.-G. Meißner, F. Stollenwerk, and A. Wirzba. Erratum to: Dispersive analysis for $\eta \to \gamma\gamma^{\star}$. *The European Physical Journal C*, 75(6):1–3, 2015.

Appendices

A Decay Kinematics

A.1 $\eta' \to \gamma\gamma$ Decay

As shown in Fig. 2a, the two photon decay can be expressed in terms of the respective momentum, $P_p(\eta') \to \gamma(\epsilon_1, p)\gamma(\epsilon_2, k)$, where ϵ_1 and ϵ_2 are the polarizations of the photons with 4-momenta p and k. Dropping the nomenclature (η') in $P_p(\eta')$, the four momentum of the decaying meson is $P_p = p + k$. Using the Feynman rules as given in [49]and [50], which are Lorentz and gauge invariant and also parity conserving, the amplitude can be solved to be:

$$\mathcal{M}(P_P \to \gamma(\epsilon_1, p)\gamma(\epsilon_2, k)) = M_P(p^2 = 0, k^2 = 0)\varepsilon_{\mu\nu\rho\sigma}\epsilon_1^\mu p^\nu \epsilon_2^\rho k^\sigma \tag{22}$$

where $\varepsilon_{\mu\nu\rho\sigma}$ is the antisymmetric metric tensor. The form factor, $M_P(p^2 = 0, k^2 = 0)$, contains information of the decaying meson and since the decay products are on-shell photons, which are massless, M_P is a constant given as;

$$M_P = \begin{cases} \dfrac{\alpha}{\pi f_\pi} & \text{if } P = \eta'; \\ \dfrac{\alpha}{\pi f_\pi}\dfrac{1}{\sqrt{3}}\left(\frac{f_\pi}{f_8}\cos\theta_{mix} - 2\sqrt{2}\frac{f_\pi}{f_0}\sin\theta_{mix}\right) & \text{if } P = \eta; \\ \dfrac{\alpha}{\pi f_\pi}\dfrac{1}{\sqrt{3}}\left(\frac{f_\pi}{f_8}\sin\theta_{mix} + 2\sqrt{2}\frac{f_\pi}{f_0}\cos\theta_{mix}\right) & \text{if } P = \eta' \end{cases} \tag{23}$$

where $\alpha = e^2/4\pi \approx 1/137$ is the fine structure constant, $f_\pi \approx 92.4\,\text{MeV}$ is the physical value of the pion-decay constant and $f_0 \approx 1.04 f_\pi$ and $f_8 \approx 1.3 f_\pi$ are the singlet and octet Pseudo-Goldstone meson decay constants.

A.1.1 *Squared Matrix Element*

The squared matrix element of the decay $P_P \to \gamma(\epsilon_1, p)\gamma(\epsilon_2, k)$ is given by

$$|\mathcal{M}(P_P \to \gamma(\epsilon_1, p)\gamma(\epsilon_2, k))|^2 = |M_P|^2 \varepsilon_{\mu\nu\rho\sigma}\varepsilon_{\mu'\nu'\rho'\sigma'}\epsilon_1^\mu p^\nu \epsilon_2^\rho k^\sigma \epsilon_1^{\mu'} p^{\nu'} \epsilon_2^{\rho'} k^{\sigma'} \tag{24}$$

which can be simplified to;

$$|\mathcal{M}(P_P \to \gamma(p)\gamma(k))|^2 = |M_P|^2 \varepsilon_{\mu\nu\rho\sigma}\varepsilon^{\mu\nu}{}_{\rho'\sigma'} p^\rho p^{\rho'} k^\sigma k^{\sigma'} \tag{25}$$

by assuming that the polarizations of the photons remain unobserved, as they are in CLAS. Therefore the photon polarization vectors can be summed

using Eq. 5.75 from [49] which reads as;

$$\sum_{polarizations} \epsilon_\mu \epsilon_{\mu'} \rightarrow -g_{\mu\mu'} \tag{26}$$

As indicated in [49], the right arrow indicates that this is not an actual equality, but the solution is valid as long as both sides are dotted into Eq. 24. The antisymmetric tensor, $\varepsilon_{\mu\nu\rho\sigma}\varepsilon^{\mu\nu}{}_{\rho'\sigma'}$ is simplified using Eq. A.30 of [49];

$$\varepsilon_{\mu\nu\rho\sigma}\varepsilon^{\mu\nu}{}_{\rho'\sigma'} = -2(g_{\rho\rho'}g_{\sigma\sigma'} - g_{\rho\sigma'}g_{\rho'\sigma}) \tag{27}$$

$$\tag{28}$$

Applying Eq. 27 to Eq. 25 results in;

$$|\mathcal{M}(P_P \rightarrow \gamma(p)\gamma(k))|^2 = |M_P|^2 \, (-2)(p^2k^2 - (p \cdot k)^2) \ . \tag{29}$$

Substituting

$$(p+k)^2 = p^2 + k^2 + 2(p \cdot k) \ , \tag{30}$$

and applying $p^2 = k^2 = 0$, since both photons are massless because they are on-shell, we can derive the final expression of the squared amplitude of the decay $P_P \rightarrow \gamma(\epsilon_1, p)\gamma(\epsilon_2, k)$ as;

$$|\mathcal{M}(P_P \rightarrow \gamma(p)\gamma(k))|^2 = |M_P|^2 \, \frac{1}{2}(p+k)^4 = \frac{1}{2} \, |M_P|^2 \, m_P^4 \tag{31}$$

where m_P^4 is the mass of the η'derived from the 4-momenta conservation equation $(p+k)^4 = m_P^4$

A.1.2 *Decay rate*

The decay rate of a two-body decay is explained in Equation 46.17 of [30] as

$$d\Gamma = \frac{1}{32\pi^2} A \, |\mathcal{M}|^2 \, \frac{|\mathbf{p_1}|}{m_p^2} d\Omega \ , \tag{32}$$

where $d\Omega$ is the solid angle of particle 1 and A is the symmetry factor which appears because of the Bose symmetry of the two outgoing photons. Substituting the square matrix element from Eq. 31 into Eq. 32 and integrating over the solid angle yields;

$$\Gamma_{P\rightarrow\gamma\gamma} = \frac{1}{32\pi^2} \frac{1}{2} \, |\mathcal{M}(P_P \rightarrow \gamma(p)\gamma(k))|^2 \, \frac{|\mathbf{p}|}{m_P^2} 4\pi = \frac{1}{32\pi} \, |M_P|^2 \, m_P^2 \, |\mathbf{p}| \tag{33}$$

Finally, in the center-of-mass (C.M.) frame of the decaying meson, $\mathbf{p} = \mathbf{E}_\gamma^{\mathbf{C.M.}} = \frac{\mathbf{m_P}}{\mathbf{2}}$, we find the final expression of the decay rate of $P_P \rightarrow \gamma(\epsilon_1, p)\gamma(\epsilon_2, k)$ as;

$$\Gamma_{P\rightarrow\gamma\gamma} = \frac{1}{64\pi} \, |M_P|^2 \, m_P^3 \ . \tag{34}$$

A.2 $\phi \to \eta\gamma$ Decay

The $\phi \to \eta\gamma$ decay is analogous to the $\eta' \to \gamma\gamma$ decay by replacing the initial pseudoscalar meson $P_p$with a vector meson V_p and one of the γ propagators with η. In this substitution

$$\mathcal{M}(V_P(\epsilon_1) \to \eta(p)\gamma(\epsilon_2, k)) = M_V(p^2 = m_\eta, k^2 = 0)\varepsilon_{\mu\nu\rho\sigma}\epsilon_1^\mu p^\nu \epsilon_2^\rho k^\sigma \tag{35}$$

again, $\varepsilon_{\mu\nu\rho\sigma}$ is the antisymmetric metric tensor and the form factor, $M_V(p^2 = \eta, k^2 = 0)$, contains information of the $\phi - \eta$ transition.

A.2.1 *Decay rate*

The algebra for solving the squared matrix element is similar to Sec. A.1.1, however since now the initial meson has polarization, a factor of $1/3$ [51] is introduced. The decay rate is also similar within a factor of $1/3$ and can be represented as:

$$\Gamma_{V\to\eta\gamma} = \frac{1}{3}\frac{1}{64\pi}\left|M_V\right|^2\left(\frac{m_\phi - m_\eta}{m_\phi}\right)^3 . \tag{36}$$

A.3 η' Dalitz Decay

When a pseudoscalar meson decays via a photon γ and a dilepton (l^+l^-) pair, it is known as a Dalitz decay or a so-called single off-shell decay. The Dalitz decay is related to the two photon decay. However, in the Dalitz decay, one of the photons is off-shell (γ^*) and decays into a dilepton pair. Since the Dalitz decay is related to the two photon decay, the form factor of the Dalitz decay, for P(η'), will be similar to the form factor of the two photon decay of P$(\ \eta')$, except there will be an effective mass dependence for the Dalitz decay. Figure 2b depicts the Feymann diagram of the Dalitz decay.

The amplitude for the decay $P_P \to \gamma^\star(p)\gamma(k) \to l^+(p_+)l^-(p_-)\gamma(k)$ is given by the following expression:

$$\mathcal{M}(P \to l^+(p_+, s_+)l^-(p_-, s_-)\gamma) = M_P(p^2, k^2 = 0)\varepsilon_{\mu\nu\rho\sigma}\frac{1}{q^2}e\bar{u}(p_-, s_-)\gamma^\mu v(p_+, s_-)q^\nu\epsilon^\rho k^\sigma. \tag{37}$$

Comparing the amplitudes of Eq. 37 and Eq. 22 it is seen that the polarization of the off-shell photon turned into the current $e\bar{u}(p_-, s_-)\gamma^\mu v(p_+, s_-)$ of the lepton pair. The parameters $s_\pm$ are the spin helicities of the outgoing leptons $l^\pm$ and as in Eq. 24, ϵ is the polarization of the outgoing photon.

A.3.1 *Squared Matrix Element*

$$\left|\mathcal{M}(P \to l^+(p_+, s_+) l^-(p_-, s_-)\gamma)\right|^2 =$$
$$\frac{e^2}{q^4} \left|M\right|^2 \varepsilon_{\mu\nu\rho\sigma}\varepsilon_{\mu'\nu'\rho'\sigma'} \bar{u}(p_-, s_-)\gamma^\mu v(p_+, s_+)\bar{v}(p_+, s_+)\gamma^{\mu'} u(p_-, s_-) q^\nu \epsilon^\rho k^\sigma q^{\nu'} \epsilon^{\rho'} k^{\sigma'}. \tag{38}$$

using an equation found between equation 5.3 and 5.4 found in [49]

$$\sum_{s_-, s_+} \bar{u}(p_-, s_-)\gamma^\mu \nu(p_+, s_+)\bar{\nu}(p_+, s_+)\gamma^{\mu'} u(p_-, s_-) = Tr\left[(\not{p}_- + m)\gamma^\mu(\not{p}_+ - m)\gamma^{\mu'}\right]$$
$$= 2q^2\left[-(g_{\mu\mu'} - \frac{p_\mu p_{\mu'}}{q^2}) - \frac{(p_+ - p_-)_\mu (p_+ - p_-)_{\mu'}}{q^2}\right] \tag{39}$$

where the identity $q = p_+ + p_-$ was used. Substituting Eq. 39 into Eq. 38

$$\left|\mathcal{M}\right|^2 = \frac{2e^2\left|M_P\right|^2}{q^2}\varepsilon_{\mu\nu\rho\sigma}\varepsilon_{\mu'\nu'\rho'\sigma'}\left[-g^{\mu\mu'} - \frac{(p_+ - p_-)^\mu (p_+ - p_-)^{\mu'}}{q^2}\right](-g^{\nu\nu'}) q^\rho k^\sigma q^{\rho'} k^{\sigma'} \tag{40}$$

Substituting $k = P - q$ and $p_- = q - p_+$ into Eq. 40

$$\begin{aligned}\left|\mathcal{M}\right|^2 =& \frac{2e^2\left|M_P\right|^2}{q^2}\varepsilon_{\mu\nu\rho\sigma}\varepsilon_{\mu'\nu'\rho'\sigma'}\left[-g^{\mu\mu'} - \frac{(2p_+ - q)^\mu (2p_+ - q)^{\mu'}}{q^2}\right] \\ &\times (-g^{\nu\nu'})(q^\rho P^\sigma - q^\rho q^\sigma)(q^\rho P^{\sigma'} - q^{\rho'} q^{\sigma'})\end{aligned} \tag{41}$$

Applying properties of $-g^{\mu\mu'}$ and $-g^{\nu\nu'}$ onto Eq. 41

$$\left|\mathcal{M}\right|^2 = \frac{2e^2\left|M_P\right|^2}{q^2}\left[\varepsilon_{\mu\nu\rho\sigma}\varepsilon^{\mu\nu}{}_{\rho'\sigma'} q^\rho P^\sigma q^{\rho'} P^{\sigma'} + \frac{4}{q^2}\varepsilon_{\mu\nu\rho\sigma}\varepsilon^{\mu}{}_{\nu'\rho'\sigma'} p_+^\nu p_+^{\nu'} q^\rho q^{\rho'} P^\sigma P^{\sigma'}\right] \tag{42}$$

Switching to the rest frame of the pseudoscalar meson, P_p, the 4-momenta is transformed to $P^\sigma = m_p \delta^{\sigma 0}$. The squared amplitude of Eq. 42 reads;

$$\left|\mathcal{M}\right|^2 = \frac{2e^2\left|M_P\right|^2}{q^2} m_p^2 \left[\varepsilon_{\mu\nu\rho}\varepsilon^{\mu\nu}{}_{\rho'} q^\rho q^{\rho'} - \frac{4}{q^2}\varepsilon_{\mu\nu\rho}\varepsilon^{\mu}{}_{\nu'\rho'} p_+^\nu p_+^{\nu'} q^\rho q^{\rho'}\right] \tag{43}$$

The sign change is due to $g^{\sigma\sigma'} = -\delta^{\sigma\sigma'}$. Using the antisymmetric tensor properties $\varepsilon_{\mu\nu\rho}\varepsilon^{\mu\nu}{}_{\rho'} = 2\delta_{\rho\rho'}$ and $\varepsilon_{\mu\nu\rho}\varepsilon^{\mu}{}_{\nu'\rho'} = \delta_{\nu\nu'}\delta_{\rho\rho'} - \delta_{\nu\rho'}\delta_{\rho\nu'} = (\hat{e}_\nu \times \hat{e}_\rho)\cdot(\hat{e}_{\nu'} \times \hat{e}_{\rho'})$, Eq. 43 is reduced to

$$\left|\mathcal{M}\right|^2 = \frac{2e^2\left|M_P\right|^2}{q^2} m_p^2 \left[2\left|\mathbf{q}\right|^2 - \frac{4}{q^2}\left|\mathbf{q}\right|^2\left|\mathbf{p}_+\right|^2 \sin^2(\theta_{p_+ q})\right] \tag{44}$$

A.3.2 *Decay rate*

The decay rate of a three-body decay is given in Equation 46.19 of [30] as

$$d\Gamma = \frac{1}{(2\pi)^5}\frac{1}{16m_p^2}\left|\mathcal{M}\right|^2\left|\mathbf{p_1^*}\right|\left|\mathbf{p_3}\right| d\Omega_1^* d\Omega_3 dm_{12} \ , \tag{45}$$

where $(|\mathbf{p_1^*}|, \Omega_1^*)$ is the momentum of particle 1 in the rest frame of 1 and 2, and Ω_3 is the angle of particle 3 in the rest frame of the decaying particle m_p [30]. Relating Eq. 45 to the variables in Eq. 44, where $(|\mathbf{p_1^*}|, \Omega_1^*) = (|\mathbf{p_+}|, \Omega_{p_+q})$, $m_{12} = q$ and $(|\mathbf{p_3}|, \Omega_3) = (|\mathbf{p_k}|, \Omega_k)$, reads;

$$d\Gamma = \frac{1}{(2\pi)^5}\frac{1}{16m_p^2}\left|\mathcal{M}\right|^2\left|\mathbf{p_+}\right|\left|\mathbf{p_k}\right| d\Omega_+ d\Omega_k dq \ , \tag{46}$$

In the rest from of the decaying particle m_p, the 3-momenta $|\mathbf{p_k}| = |\mathbf{q}|$ and the solid angle $\Omega_k = \Omega_q$. Substituting the square matrix element from Eq. 44 into Eq. 46 yields;

$$d\Gamma = \frac{1}{(2\pi)^5}\frac{1}{16m_p^2}\frac{2e^2\left|M_P\right|^2}{q^2}m_p^2\left[2\left|\mathbf{q}\right|^2 - \frac{4}{q^2}\left|\mathbf{q}\right|^2\left|\mathbf{p_+}\right|^2\sin^2(\theta_{p_+q})\right]\left|\mathbf{p_+}\right|\left|\mathbf{q}\right| d\Omega_{p_+q} d\Omega_q dq \ . \tag{47}$$

The variables $|\mathbf{q}|$ and $|\mathbf{p_+}|$ can be redefined, by means of Eq. 46.20b and Eq. 46.20a of [30], as

$$\left|\mathbf{q}\right| = \frac{m_p^2 - q^2}{2m_p} \tag{48}$$

$$\left|\mathbf{p_+}\right| = \frac{\sqrt{q^2 - 4m_l^2}}{2} = \frac{q\sqrt{1 - \frac{4m_l^2}{q^2}}}{2} = \frac{q\mathcal{K}}{2} \ , \tag{49}$$

where $\mathcal{K} = \sqrt{1 - \frac{4m_l^2}{q^2}}$. Replacing the variables calculated in Eq. 48 and Eq. 49 into Eq. 47 and collecting terms yields;

$$d\Gamma = \frac{1}{(2\pi)^5}\frac{1}{16m_p^2}\left|M_P\right|^2\left[\frac{2e^2m_p^2}{8}\left(\frac{m_p^2 - q^2}{2m_p}\right)^3\right]\left(2 - \mathcal{K}^2\sin^2(\theta_{p_+q})\right)\frac{\mathcal{K}}{4q^2}dq^2 d\Omega_{p_+q} d\Omega_q \ , \tag{50}$$

where the identity $qdq = \frac{dq^2}{2}$. Performing the integration of $\Omega_{p_+q} d\Omega_q$ and replacing $e^2 = 4\pi\alpha$ transforms Eq. 50 into;

$$d\Gamma = \frac{1}{(2\pi)^3}\frac{1}{32}\frac{4\pi\alpha}{3}\left|M_P\right|^2\left[\frac{m_p^6\left(1 - \frac{q^2}{m_p^2}\right)^3}{m_p^3}\right]\left(3 - \mathcal{K}^2\right)\frac{\mathcal{K}}{q^2}dq^2 \ , \tag{51}$$

which can be simplified further to;

$$d\Gamma = \left(\frac{1}{64\pi}\left|M_P\right|^2 m_P^3\right)\frac{2\alpha}{3\pi}\frac{1}{q^2}\left(1-\frac{q^2}{m_p^2}\right)^3\left(1+\frac{2m_l^2}{q^2}\right)\left(1-\frac{4m_l^2}{q^2}\right)^{\frac{1}{2}} dq^2 \ . \tag{52}$$

It can be seen that the first set of variables in parenthesis in Eq. 52 is Eq. 34, therefore;

$$\frac{d\Gamma}{\Gamma_{\gamma\gamma}dq^2} = \frac{2\alpha}{3\pi}\frac{1}{q^2}\left(1-\frac{q^2}{m_p^2}\right)^3\left(1+\frac{2m_l^2}{q^2}\right)\left(1-\frac{4m_l^2}{q^2}\right)^{\frac{1}{2}} \tag{53}$$

which is the Kroll-Wada equation founded in [25].

A.4 ϕ Dalitz Decay

The amplitude for the decay $V_P \to \gamma^\star(p_1)\eta(p_2) \to l^+(p_+)l^-(p_-)\eta(p_2)$ is similar Eq. 37, but replacing the on-shell photon with an η:

$$\mathcal{M}(P \to l^+(p_+,s_+)l^-(p_-,s_-)\eta(p_2)) = M_P(p_1^2,p_2^2)\varepsilon_{\mu\nu\rho\sigma}\frac{1}{q^2}e\bar{u}(p_-,s_-)\gamma^\mu v(p_+,s_-)q^\nu\epsilon^\rho p_2^\sigma. \tag{54}$$

A.4.1 *Decay rate*

The decay rate for the ϕ transition to $\eta\gamma^\star$ is derived as [28]:

$$\frac{d\Gamma}{\Gamma_{\eta\gamma}dq^2} = \frac{\alpha}{3\pi}\frac{1}{q^2}\left(\left(1+\frac{q^2}{m_\phi^2-m_\eta^2}\right)^2-\frac{4m_\phi^2q^2}{m_\phi^2-m_\eta^2}\right)^{\frac{3}{2}}\left(1+\frac{2m_l^2}{q^2}\right)\left(1-\frac{4m_l^2}{q^2}\right)^{\frac{1}{2}} \ , \tag{55}$$

B Tabular Rates

Table 1 gives expected count rate for several bins of $M(e^+e^-)$ for a torus field setting of 75%. Table 2 gives expected count rate for several bins of $M(e^+e^-)$ for a torus field setting of 100%.

$M(e^+e^-)$ Bin Center	Upper	Uncertainty	Lower	Uncertainty
0.01	8924	94	946	31
0.03	1720	41	180	13
0.05	1041	32	113	11
0.07	758	28	84	9
0.09	578	24	62	8
0.11	479	22	54	7
0.13	411	20	45	7
0.15	369	19	37	6
0.17	329	18	36	6
0.19	317	18	36	6
0.21	280	17	30	5
0.23	268	16	28	5
0.25	250	16	26	5
0.27	269	16	28	5
0.29	266	16	24	5
0.31	250	16	25	5
0.33	240	15	24	5
0.35	258	16	25	5
0.37	309	18	31	6
0.39	280	17	28	5
0.41	352	19	35	6
0.43	285	17	31	6
0.45	299	17	31	6
0.47	315	18	34	6
0.49	328	18	35	6
0.51	326	18	38	6
0.53	331	18	30	5
0.55	282	17	28	5
0.57	401	20	38	6
0.59	416	20	45	7
0.61	438	21	48	7
0.63	445	21	44	7
0.65	448	21	44	7
0.67	577	24	63	8
0.69	689	26	69	8
0.71	728	27	79	9
0.73	716	27	71	8
0.75	706	27	73	9
0.77	565	24	54	7
0.79	277	17	29	5
Total	26521	163	2784	53

Table 1: Counts rates for bins of $M(e^+e^-)$ at 75% torus field

$M(e^+e^-)$ Bin Center	Upper	Uncertainty	Lower	Uncertainty
0.01	7937	89	859	29
0.03	1516	39	163	13
0.05	934	31	102	10
0.07	684	26	77	9
0.09	501	22	56	7
0.11	392	20	45	7
0.13	366	19	40	6
0.15	335	18	34	6
0.17	276	17	31	6
0.19	266	16	30	5
0.21	246	16	28	5
0.23	238	15	25	5
0.25	218	15	22	5
0.27	245	16	26	5
0.29	225	15	21	5
0.31	218	15	22	5
0.33	217	15	22	5
0.35	226	15	23	5
0.37	275	17	29	5
0.39	256	16	27	5
0.41	292	17	31	6
0.43	274	17	29	5
0.45	262	16	26	5
0.47	244	16	27	5
0.49	296	17	32	6
0.51	303	17	36	6
0.53	295	17	28	5
0.55	255	16	26	5
0.57	338	18	33	6
0.59	381	20	43	7
0.61	382	20	43	7
0.63	399	20	41	6
0.65	419	20	41	6
0.67	527	23	57	8
0.69	597	24	62	8
0.71	695	26	76	9
0.73	664	26	68	8
0.75	657	26	68	8
0.77	545	23	54	7
0.79	271	16	28	5
Total	23667	154	2528	50

Table 2: Counts rates for bins of $M(e^+e^-)$ at 100% torus field